NIORD: A COMPACT HIGH-RESOLUTION LOW-LIGHT IMAGER FOR MARINE TRAFFIC SURVEILLANCE

Eric RUCH, Alexandre BOUEE [(1)], Xavier BOZEC [(1)], Jean-Louis CAREL [(1)], Christophe CLOUTRIER [(1)], Josselin COUPARD [(1)], François RIGUET [(1)], Océane ROURE [(1)], Olivier THEBAULT [(1)], Valentin VIEILLOT [(1)]

[(1)] SAFRAN Reosc, Avenue de la Tour Maury, 91280 Saint-Pierre-du-Perray, France
Email: eric.ruch@safrangroup.com

KEYWORDS: NorSat-4, microsatellite, optronics, imaging system, New Space, surveillance, low-light, optics, sensors, baffle, stray light, compact, catadioptric, slanted edge, ship-tracking

ABSTRACT:

NIORD is a compact high-resolution low-light imager for marine traffic surveillance. It will be used by the Norwegian Defense Research Establishment (FFI) on the NorSat-4 satellite, which is owned by the Norwegian Space Agency. This imager is based on a catadioptric optical design fully integrated at SAFRAN Reosc. Its integration on the spacecraft was performed in May 2023 at UTIAS Space Flight Laboratory. This paper develops the project life cycle, from the opto-mechanical design to the integration process and tests performed on the instrument.

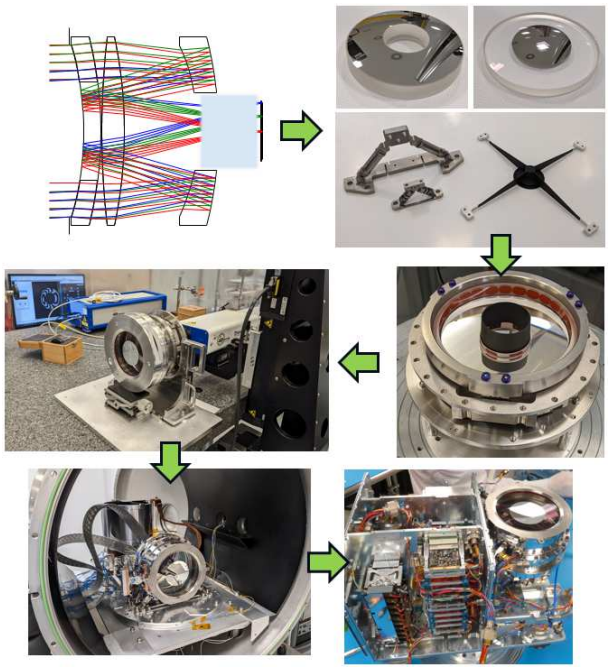

Figure 1. NIORD project lifecycle illustrated by pictures

1. INSTRUMENT AND SPECIFICATIONS

NIORD imager will be used by the Norwegian Defense Research Establishment (FFI) on the NorSat-4 satellite [1] dedicated to the surveillance of the seas and marine traffic. For this mission, FFI has selected the SEEING 130 imager developed by SAFRAN Reosc.
The instrument will provide a ground sampling distance of 10 m at an orbit altitude of 600 km. The main optical requirement is to achieve an in-orbit contrast better than 10% at Nyquist frequency (including the detector contribution) over the entire field of view (FoV) of 65x43 km². In addition, the differential distortion has to be smaller than the pixel size (5.5 µm) because the instrument is operating in time delay integration (TDI) mode. A compact design is required to fit into a small volume of 240x190x200 mm³ (without the outer baffle). Finally, the total mass of the imager is less than 9 kg and the required power 25 W.

2. OPTO-MECHANICAL DESIGN

NIORD imager is a catadioptric lens featuring an entrance doublet, a Mangin mirror and a 5-lens field corrector (see Fig. 2). The use of several aspherical surfaces allows diffraction-limited performance over the full field of view in a very compact design. The optical components are mounted in individual barrels using a space qualified bonding process and the assembled lenses are then fitted into a titanium structure that interfaces to the spacecraft platform via three bipods.

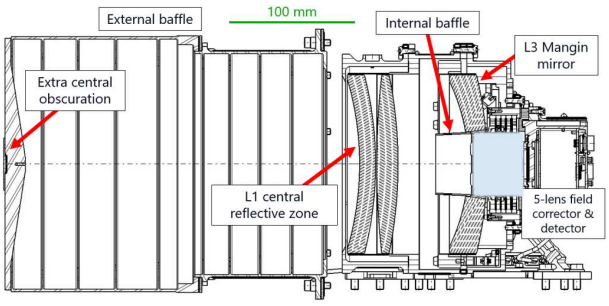

Figure 2. NIORD opto-mechanical design

To keep optimal performance over the 22 ± 4°C

thermal range, the optical design has been carefully athermalized to limit the defocus introduced by the change of refractive indices and the expansion of the lenses. Depending on the functional conditions, the impact of thermal gradients has also been computed. It appears that a few points of contrast could be lost, but the performance still stays within the margin allocated to this contributor.

3. BAFFLING AND STRAY LIGHT

Due to the original optical design, a specific baffling has been developed to suppress stray light. A classical front baffle with vanes along with an internal conical baffle have been implemented.

An additional frontal blocking area is also needed to prevent some large-angle rays to go to the detector through a quadruple reflection in the lenses (see Fig. 3).

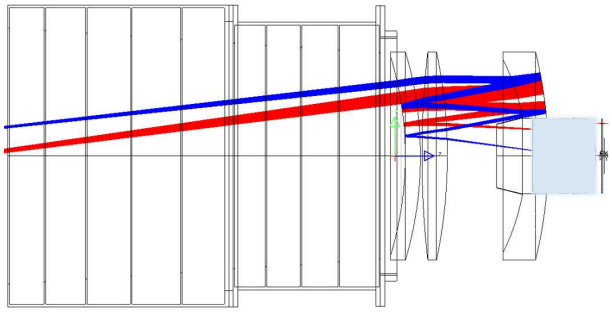

Figure 3. Problematic quadruple reflection

Optical design is optimized regarding stray light coming from ghosts. Ghosts level is below -40 dB relative to the useful signal over the full FoV. Calculated patterns are shown on Fig. 4, 5 and 6.

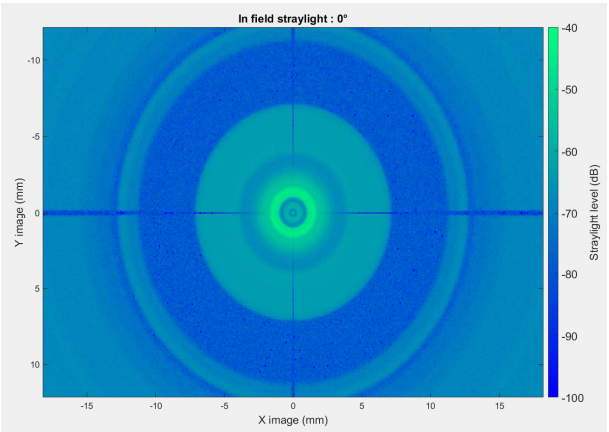

Figure 4. Ghost level on axis

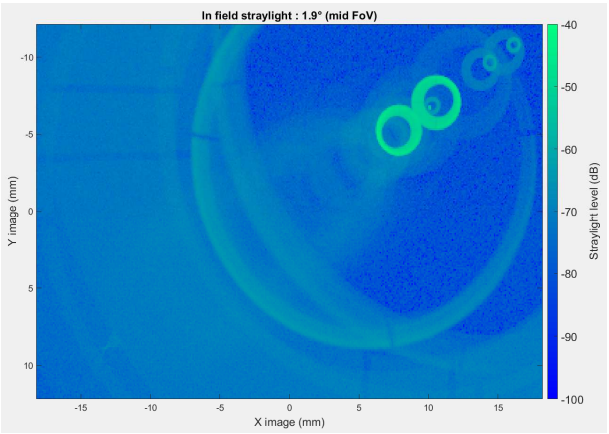

Figure 5. Ghost level at mid FoV

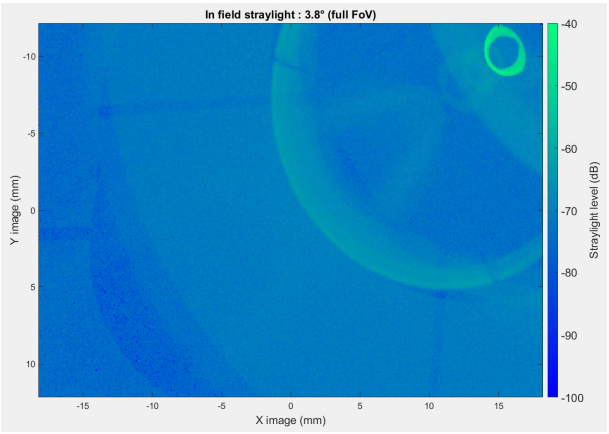

Figure 6. Ghost level at full FoV

Several stray light scenarios were also calculated such as the contribution from the sun (direct and glint), the contribution from the clouds and from the moon during night-time. Data used for applied black coating BRDF are directly coming from measurements performed by the optical department of CNES [2].

The point source transmittance (PST), which is equal to the amount of stray light on the focal plane divided by the amount of light incident at the entrance aperture of the system, was computed on LightTools software. The instrument calculated PST is given on Fig. 7.

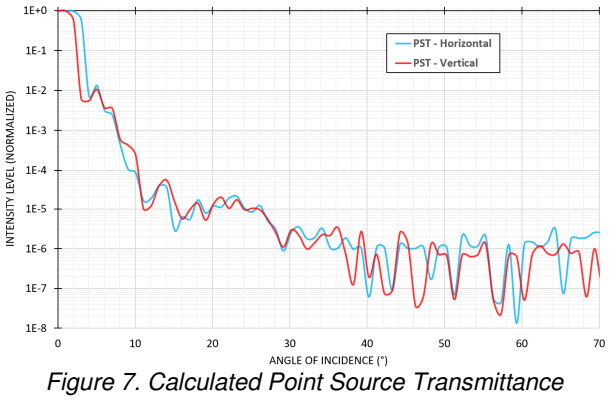

Figure 7. Calculated Point Source Transmittance

Note that the PST is not exactly the same following horizontal and vertical axis because the FoV of the instrument is rectangular. Whereas the beginning of the curves (below 2.11° in vertical direction and 3.15° in horizontal direction) are related to the useful signal, the other peaks can be related to stray light contributors such as baffles, lenses edges or mechanical parts. Above an incidence angle of 26°, the stray light is drastically reduced because of the exclusion angle of the external baffle.

4. PARTS MANUFACTURING AND COATINGS

The individual components inside the instrument mostly come from France and Germany:

- All the lenses were manufactured by Asphericon
- Lenses coatings were performed at SAFRAN Reosc for both protected silver and anti-reflective coatings
- Mechanical parts were manufactured by various French companies, a significant portion by ACMO Precision
- Black coatings on mechanical parts are from MAP Space Coatings

Each surface has been coated with in-house high performance anti-reflection (AR) coatings, along with protected silver coatings for the mirrors. An average transmission over 73% is fulfilled on the complete spectral range [400-900] nm.

As illustration, the Fig. 8 shows L1 and L3 lenses after coating. One can clearly see the central reflective zone on L1 lens that can be compared to an M2 mirror inside the optical design. On its side, L3 lens is comparable to a primary mirror within the optical design. It is AR coated on front side and protected silver coated on backside.

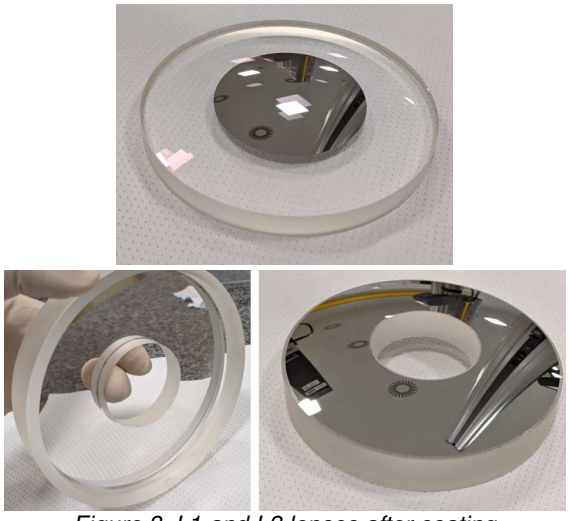

Figure 8. L1 and L3 lenses after coating

Regarding mechanical parts, the Fig. 9 shows bipods flexures and the extra obscuration in front of the external baffle after applying black coating on it (MAP PU1 from MAP Space Coatings).

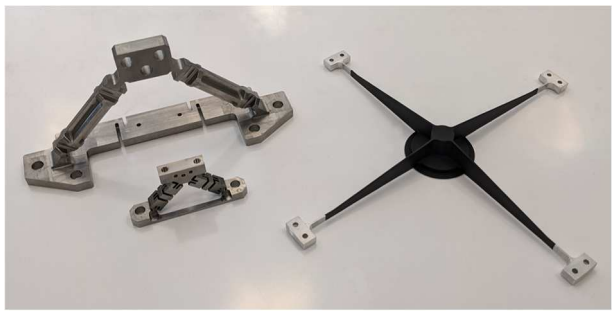

Figure 9. Bipods flexures and external baffle extra obscuration

5. INTEGRATION PROCESS

The integration of the instrument, from optical elements to the detector, was fully performed at SAFRAN Reosc. Thanks to the high-precision capabilities of SAFRAN Reosc, all the lenses have been integrated with tilts and decenters below 10 µm.

The integration method depends on the considered lens. Regarding the field corrector lenses, all the components were bonded inside individual barrels with RTV glue. Then, the barrels were machined to correct both alignment error introduced during bonding process and the wedge of the manufactured lens. Finally, all the barrels are fitted inside a titanium body. The integrated field corrector is shown on the Fig. 10.

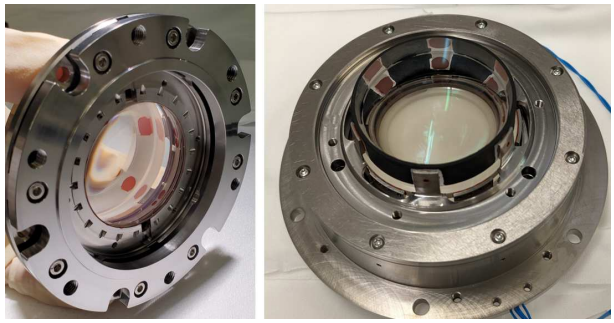

Figure 10. Flat field corrector after integration

Concerning large lenses, the alignment was directly performed during bonding process.

Bonding process of L1 and L2 lenses on TriOptics is shown on Fig. 11, whereas L3 assembly with its internal baffle is shown on Fig. 12.

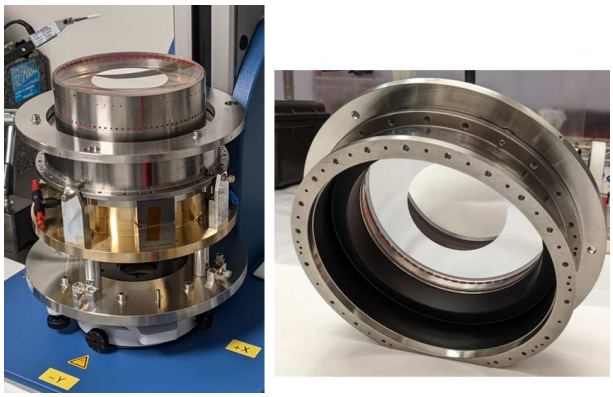

Figure 11. L1 and L2 lenses during bonding process on TriOptics

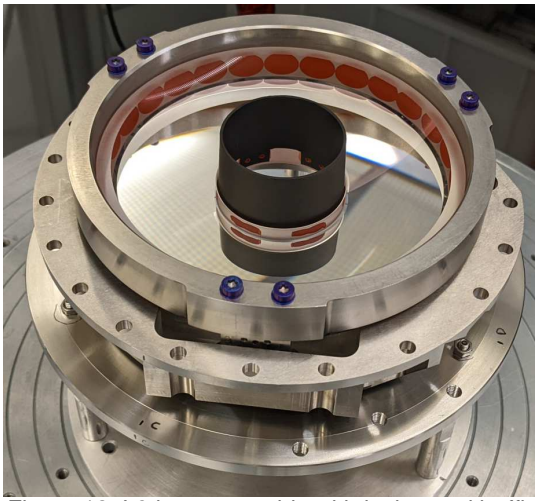

Figure 12. L3 lens assembly with its internal baffle

6. WFE TEST BENCH

A custom WFE test setup was used for both validate the performance of the optics and the alignment of the two assemblies: on one side L1 and L2 lenses assembly and on the other L3 and field corrector assembly.
WFE testing is performed in double pass at 633 nm over the full instrument FoV with motorized stages.

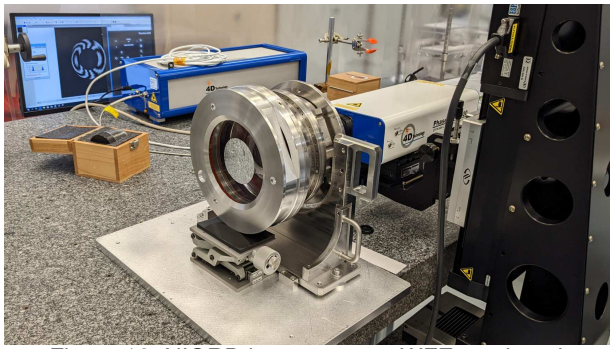

Figure 13. NIORD instrument on WFE test bench

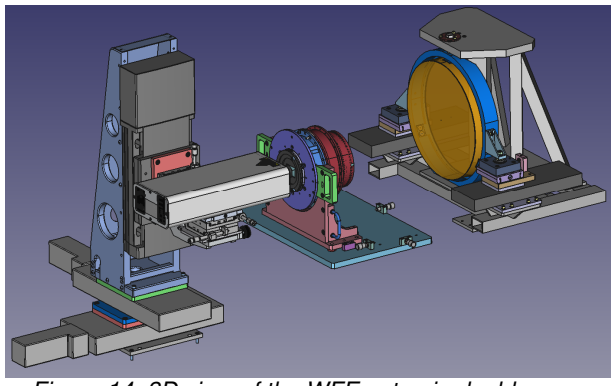

Figure 14. 3D view of the WFE setup in double pass

The optical system WFE was measured at 9 different FoV points to get 9 different WFE maps. Those maps were then fitted with annular Zernike polynomials to deduce key parameters for alignment:

- The thickness and wedge of the shim to be inserted between the groups
- The decenter to apply between groups before tightening the screws
- The residual WFE that cannot be corrected by alignment between groups

The problem consists in resolving the matrix equation Eq. 1:

Eq. 1 $$SC = M$$

Where:

- S is the matrix containing the sensitivities of the optical design to small perturbations (decenters and tilts).
- C is the compensation matrix containing the displacements to apply in order to get the best WFE. It is the matrix to be calculated.
- M is the matrix containing the measured data set.

$$\begin{matrix} \delta x_{L12} & \dots & \delta\beta_{IMAGE} \\ \downarrow & & \downarrow \end{matrix}$$

$$\begin{bmatrix} S1_{Z4/F1} & \dots & S7_{Z4/F1} \\ \dots & \dots & \dots \\ S1_{Z11/F1} & \dots & S7_{Z11/F1} \\ S1_{Z4/F2} & \dots & S7_{Z4/F2} \\ \dots & \dots & \dots \\ S1_{Z11/F25} & \dots & S7_{Z11/F25} \end{bmatrix} \times \begin{bmatrix} \delta x_{L12} \\ \delta y_{L12} \\ \delta z_{L12} \\ \delta \alpha_{L12} \\ \delta \beta_{L12} \\ \delta \alpha_{IMAGE} \\ \delta \beta_{IMAGE} \end{bmatrix} = \begin{bmatrix} \delta WFE_{Z4/F1} \\ \dots \\ \delta WFE_{Z11/F1} \\ \delta WFE_{Z4/F2} \\ \dots \\ \delta WFE_{Z11/F25} \end{bmatrix}$$

Eq. 2

Both sensitivities and measurements maps are fitted with annular Zernike polynomials terms up to Z11 for alignment correction. High order terms are not involved in compensation because alignment correction only involves low order terms. By calculating the pseudo inverse of S matrix (which is the solution to the least-squares problem), one can obtain the displacements to apply:

Eq. 3 $$C = S^{\dagger}M$$

Final measured WFE maps as well as an example of fitting result obtained with Zernike polynomials are illustrated on Fig. 15 and 16.

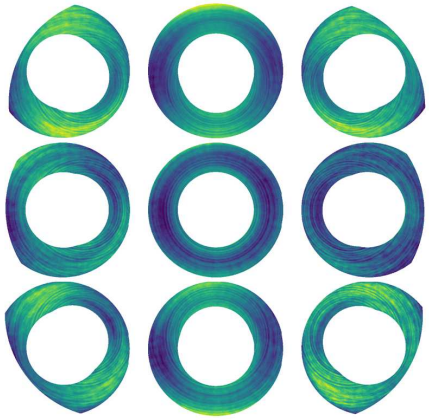

Figure 15. Measured WFE maps over FoV

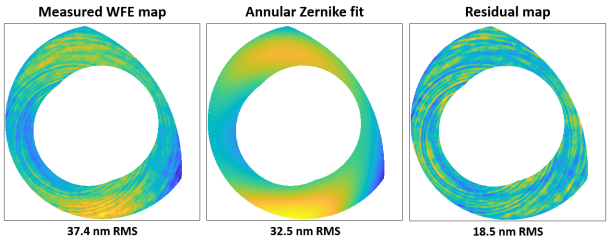

Figure 16. Example of fitting with annular Zernike polynomials

Because the as-built optical model on CodeV also contains the polishing error maps on each diopter, the correlation between the model and the measured WFE maps is extremely good. Four WFE maps are compared as information on the Fig. 17.

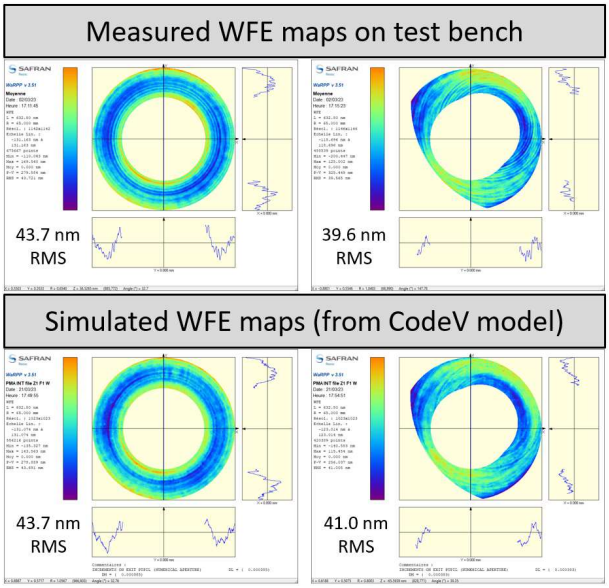

Figure 17. Comparison between measured and simulated WFE maps

The alignment accuracy and tight polishing tolerances have allowed SAFRAN Reosc to achieve a wavefront error between 24 and 67 nm RMS over the full field of view.

7. MTF TESTING

NIORD modulation transfer function was measured for both validating the performance of the full instrument (including the detector) and for the alignment of the detector with respect to optical elements.
The setup used for MTF testing is a reflective collimator projecting a slanted edge pattern towards the instrument. This slanted edge is then re-imaged by the instrument on its detector and the full MTF is calculated according to ISO 12233 [3].

Because the as-built optical model WFE is very well correlated with the measured instrument WFE (see §6), the MTF results given by CodeV were compared to MTF measurements for crosscheck.
Again, we see an extremely good correlation between MTF curves, especially near the Nyquist frequency at 91 cycles/mm (see Fig. 18).

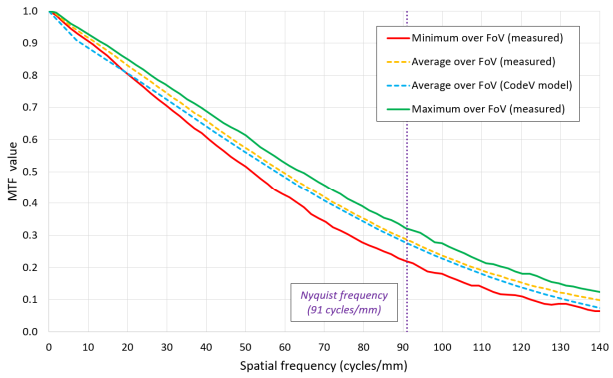

Figure 18. Measured MTF and comparison with CodeV model

Measured MTF goes from 0.22 to 0.32, including the detector, at Nyquist frequency. Those results are better than expected and provide some margin for the satellite's thermal environment.

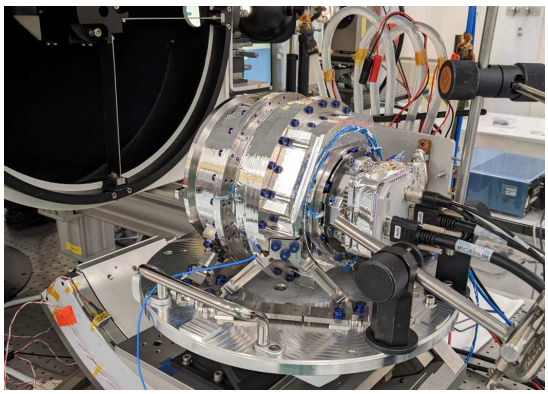

Figure 19. NIORD instrument on MTF test bench

To confirm the performance of the instrument under vacuum and thermal environment, MTF measurements have also been performed under vacuum. The MTF test bench was moved just in front of a thermal vacuum chamber (TVAC) as shown on the Fig. 20.

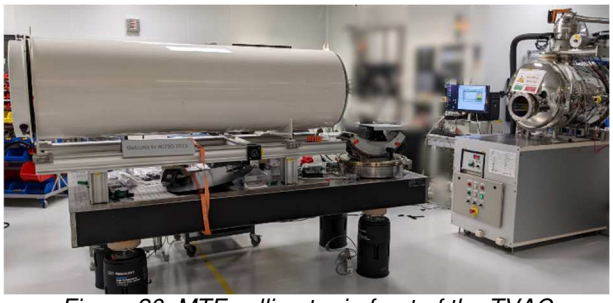

Figure 20. MTF collimator in front of the TVAC

The introduced defocus under vacuum (due to refractive index change of optical elements) was the one expected from the simulations. Moreover, the MTF results obtained on the specified thermal range T = 22 ± 4 °C show that the instrument is properly athermalized by design.

8. THERMAL CYCLING AND VIBRATIONS

The qualification sequence performed on the instrument includes thermal cycling and vibrations tests. Thermal cycling under vacuum was successfully performed between -30°C and +70°C. NIORD instrument and its external baffle inside the TVAC are shown on Fig. 21.
Moreover, an additional thermal cycling under dry nitrogen was performed on the external baffle because its thermal environment is not exactly the same as the instrument. This second thermal cycling range is in between -55°C and +110°C.

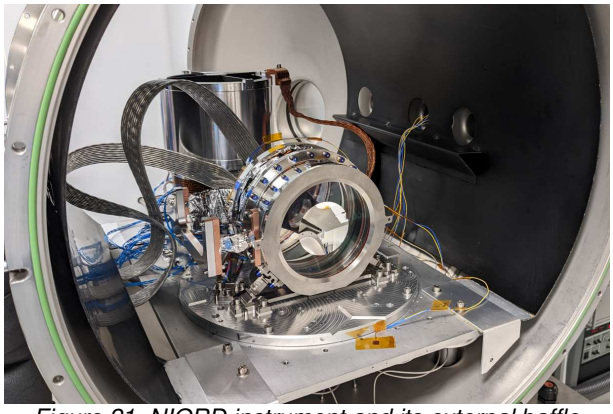

Figure 21. NIORD instrument and its external baffle inside the TVAC

Regarding the vibrations tests, because the instrument and the external baffle are mounted on separated panels on the satellite, two separated vibrations campaigns have been performed. Depending on the considered axis, the levels for random vibrations are in between 10 and 26 g RMS.

NIORD instrument and its vibration baseplate as well as the vibration shaker are shown on Fig. 22.

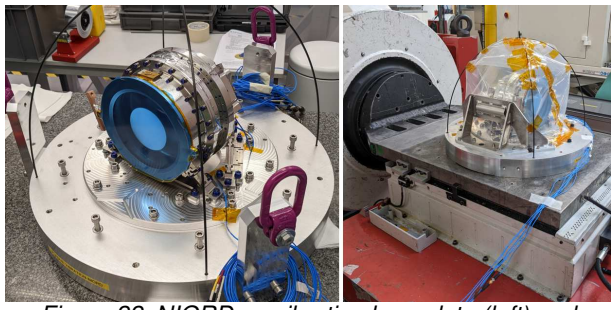

Figure 22. NIORD on vibration baseplate (left) and vibration shaker used during tests (right)

9. INTEGRATION ON NORSAT-4 SPACECRAFT

The instrument has been integrated on NorSat-4 spacecraft during the month of May 2023 at UTIAS Space Flight Laboratory located in Toronto. The instrument was integrated on DEFIANT platform [4] whose exterior and interior layouts are shown on Fig. 23 and 24.

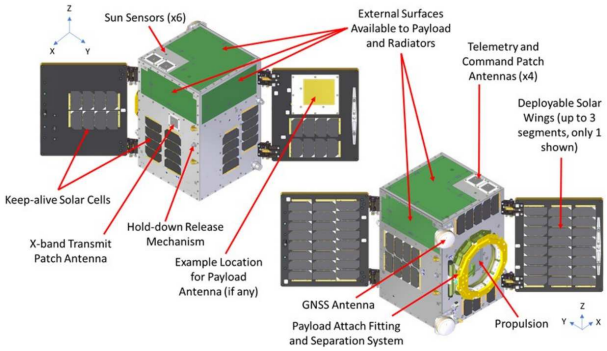

Figure 23. Spacecraft exterior layout

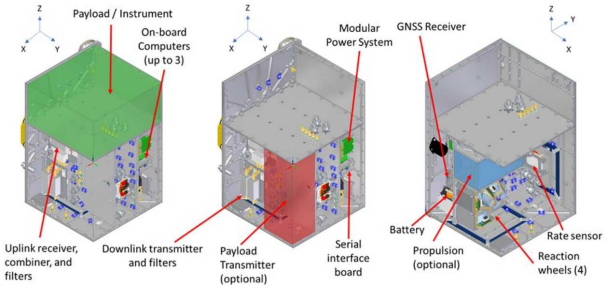

Figure 24. Simplified interior layout

This spacecraft carries an automatic identification system (AIS) ship-tracking receiver developed by Kongsberg Seatex (just as NorSat-3 did [5]) and NIORD low-light imager developed by SAFRAN Reosc (see [6] and [7]).

NIORD imager after its integration on the spacecraft is shown on the Fig. 25.

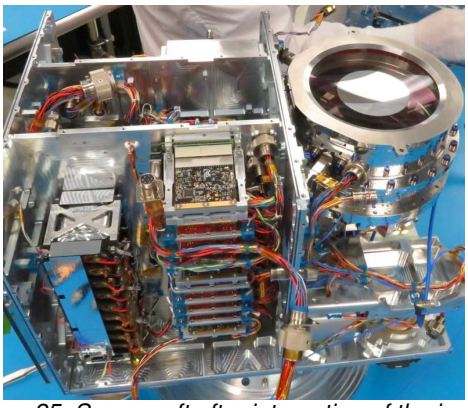

Figure 25. Spacecraft after integration of the imager

Just in front of the first lens, a motorized shutter was added by UTIAS SFL to prevent any damage coming from direct sun illumination. Fig. 26 shows this shutter on the panel in front of the instrument.

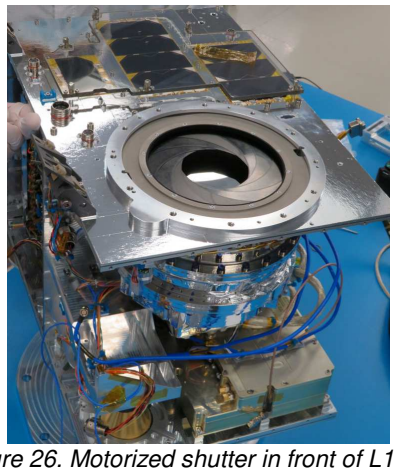

Figure 26. Motorized shutter in front of L1 lens

After adding a large quantity of electronics components, the external baffle was integrated on the front satellite panel, as shown on Fig. 27.

The full assembly was then mounted on a handling structure to facilitate its displacement. It was especially useful for MTF measurements at satellite level using the on-board electronics acquisition system.
A full qualification sequence was successfully performed at satellite level

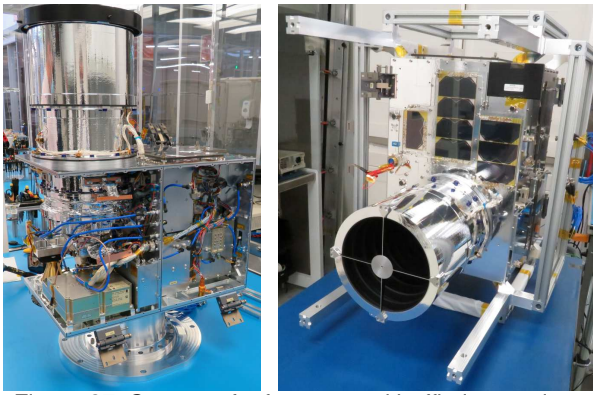

Figure 27. Spacecraft after external baffle integration (left) and full spacecraft on its handling structure (right)

10. FIRST IMAGES

The satellite was launched from Vandenberg on January, 14 2025 on board Space X Transporter-12.

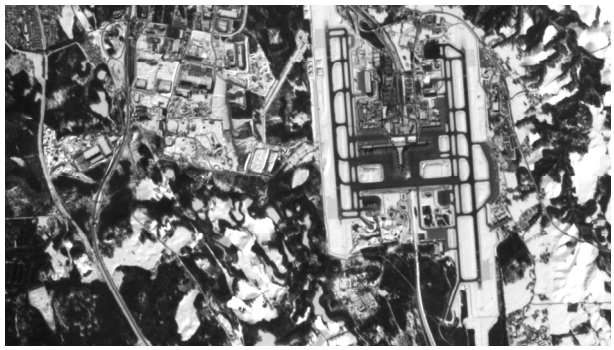

Figure 28. View from Oslo

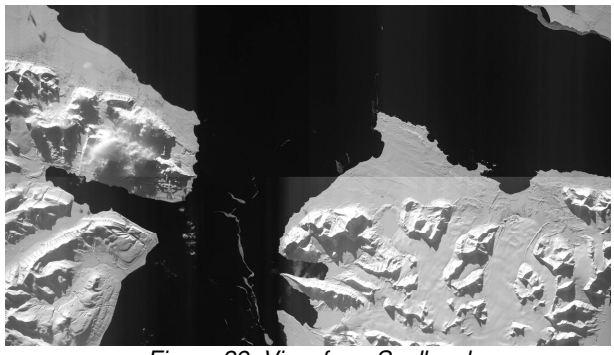

Figure 29. View from Svalbard

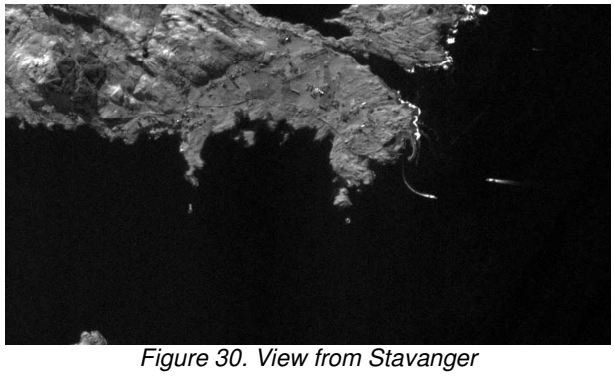

Figure 30. View from Stavanger

A new product currently under development at SAFRAN Reosc, SEEING 230 Ident, will benefit from the technologies involved during NIORD project.

11. REFERENCES

1. FFI Norwegian Defence Research Establishment, “Research and development plan 2021-2024” (2021)

2. Reymond S., Sierra G., Guillaumon O., Remaury S., Nabarra P., Combes H., Laurent E. (2012). Developpment of green paints, MAP® AQ PU1 and MAP® AQ PUK.

3. Photography–Electronic Still Picture Cameras–Resolution Measurements, ISO Standard 12233:2023

4. Larouche B., “DEFIANT: A small mass-producible microsatellite platform for demanding applications under extreme cost and size constraints,” in Small Satellites, System Services Symposium (4S), 2018

5. Skauen A., Jahnsen B., Smestad T., Grimstvedt E., Gulbrandsen F., Svenes K., Cotton B., Zee R., Blindheim E., Harr J., Rosshaug H., Kristiansen K., Storesund F., “NorSat-3 – next generation Norwegian maritime surveillance”, 33rd Annual AIAA/USU, Conference on Small Satellites (2019)

6. Bouée A., Bozec X., Carel J-L., Cloutrier C., Coupard J., Plainchamp B., Riguet F., Roure O., Thébault O., Vieillot V., "NIORD: a compact high-resolution low-light imager for marine traffic surveillance," Proc. SPIE 12798, International Optical Design Conference 2023, 1279830 (14 September 2023) ; https://doi.org/10.1117/12.2692561

7. Ruch E., "Recent developments of space optics at Safran Reosc ," Proc. SPIE 12777, International Conference on Space Optics — ICSO 2022, 127771M (12 July 2023) ; https://doi.org/10.1117/12.2689658